Environmental Science & Technology

pubs.acs.org/est Article

Arsenic Impurity in Flue Gas Significantly Inhibiting N_2O Byproduct Formation on the Chromium-Poisoned $V_2O_5-WO_3/TiO_2$ Catalyst in the NH_3-SCR Reaction

Ruihua Wang, Ziyi Fan, Jingtao Wang, Zhisu Liu, Hao Cheng, Xingshen Yang, Weixin Zou,* Wei Nie, and Lin Dong*

Cite This: *Environ. Sci. Technol.* 2025, 59, 23602−23611

Read Online

ACCESS | Metrics & More | Article Recommendations | Supporting Information

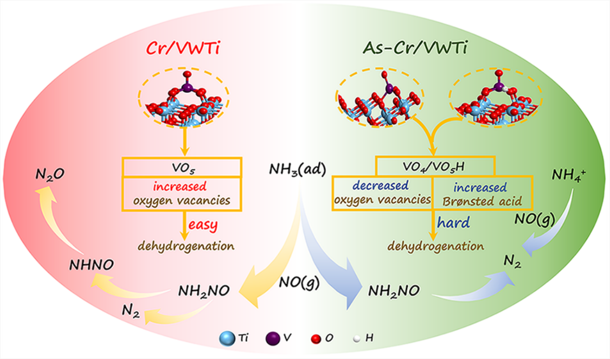

ABSTRACT: The chromium (Cr) impurity in flue gas often leads to the undesirable byproduct of the greenhouse gas N_2O in the NH_3-SCR reaction. Herein, an interesting phenomenon is first reported. Arsenic (As), as another impurity, markedly suppresses N_2O generation over the Cr-poisoned $V_2O_5-WO_3/TiO_2$ (Cr/VWTi) catalyst, especially reducing by nearly 10 times at 300 °C in NH_3-SCR. Characterizations show that the introduction of As induces the interaction between Cr and As, which inhibits the Cr incorporation into the TiO_2 lattice and promotes the transformation of monomeric VO_x species from VO_5 (Cr/VWTi) to VO_4 and VO_5H (As−Cr/VWTi). *In situ* DRIFTS and calculations demonstrate that due to the structural changes in Cr/VWTi, As−Cr/VWTi exhibits reduced oxygen vacancies as well as increased VO_4 species and Brønsted acid sites, which makes the dehydrogenation of the NH_2NO^* intermediate more difficult, resulting in lower N_2O formation during the NH_3-SCR reaction. This work provides new insights into N_2O suppression from flue gas impurities.

KEYWORDS: *NH_3-SCR, N_2O suppression, Cr & As, VWTi catalyst*

1. INTRODUCTION

The selective catalytic reduction of NO_x with NH_3 (NH_3-SCR) technology is the most widely used technology for the abatement of NO_x from stationary sources.[1−3] VWTi catalysts have been accepted as commercial NH_3-SCR catalysts for several decades.[4] During the NH_3-SCR process, N_2O, as the third most important long-lived greenhouse gas, could inevitably be generated on V-based catalysts.[4,5] The previous study has demonstrated that when the temperature is lower than 300 °C, N_2O is mainly formed from the decomposition of NH_4NO_3, while at higher temperatures, NH_3 is oxidized to form NH by the V active site and then reacts with NO to produce N_2O.[4] Moreover, two N atoms of N_2O separately come from NH_3 and NO, while the sources of the O atom in N_2O are NO, O_2, and catalyst oxygen (∼50, ∼30, and ∼20%, respectively).[6−9] Zhu et al. suggested that surface VO_x sites of the VWTi catalyst are active for N_2O formation, and the rate-determining step is related to the NH bond breaking of NH_3, which is consistent with the DFT calculation.[9,10] The bond breaking of NH_3 directly depends on the oxidation ability of the catalyst; the stronger the oxidation ability of the catalyst, the easier it is for NH_3 to deeply dehydrogenate to generate N_2O.[11,12]

Generally, SCR catalysts are used in a complex flue gas environment under operating conditions. Xing et al. has found that the chromium (Cr) deposition on V_2O_5/TiO_2 remarkably promotes N_2O formation without changing NO_x conversion, which is resulted from an increase in the V^{5+} content of the catalyst.[2] However, multiple flue gas impurities in actual working environments usually coexist and interact with each other on the catalyst, leading to the unpredictable N_2O formation performance.[13] In general, the incorporation of acidic species, particularly Brønsted acids, into the catalyst can reduce the redox capability of the catalyst, thereby effectively decreasing the N_2O byproducts.[11,14−20] Previous studies have elucidated that H_2O and SO_2 suppress N_2O formation through the enhanced Brønsted acidity and reduced redox properties.[12,21] As another main impurity, arsenic (As) is also a severe poison to commercial VWTi catalysts, typically present as As_2O_3 in flue gas with concentrations ranging from 1 $\mu g/m^3$ to

Received: July 3, 2025
Revised: October 16, 2025
Accepted: October 17, 2025
Published: October 23, 2025

https://doi.org/10.1021/acs.est.5c08985
Environ. Sci. Technol. 2025, 59, 23602−23611

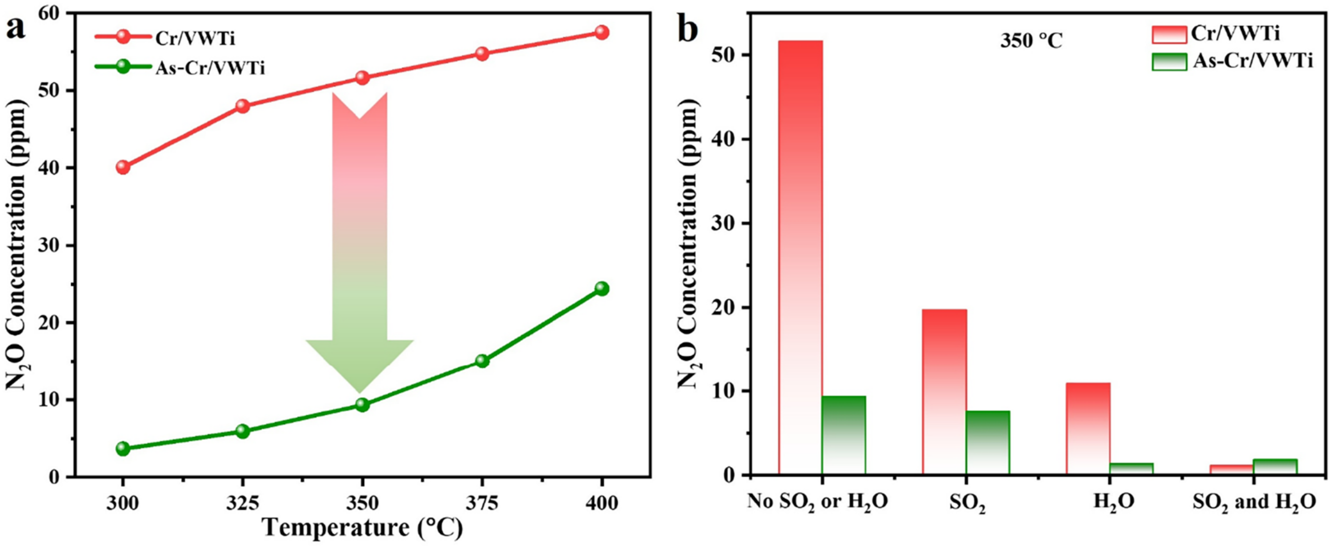

Figure 1. (a) N_2O formation of Cr/VWTi and As−Cr/VWTi in the NH_3−SCR reaction. (b) N_2O formation over Cr/VWTi and As−Cr/VWTi, with SO_2 (denoted as "SO_2"), H_2O (denoted as "H_2O"), and SO_2 and H_2O (denoted as "SO_2 and H_2O") at 350 °C. Reaction conditions: 300 ppm of NH_3, 300 ppm of NO, 4 vol % O_2, 100 ppm of SO_2 (when used), 5 vol % H_2O (when used), flow rate = 100 mL·min^{-1}, WHSV = 60,000 mL·g^{-1}·h^{-1}, and Ar as the balance.

10 mg/m^3.[22] It has been confirmed that As can form As−OH as new Brønsted acid sites for As-poisoned VWTi catalysts.[22,23] Moreover, V^{5+} in As-poisoned V_2O_5(-MoO_3)/TiO_2 oxidizes As^{3+} to As^{5+},[24,25] while Cr^{6+} in Cr-poisoned V_2O_5/TiO_2 oxidizes V^{4+} to V^{5+}.[2] Hence, when As and Cr codeposit on the VWTi catalyst surface, Cr^{6+} may be reduced to Cr^{3+} by oxidizing As^{3+} to As^{5+}, weakening the redox property of the Cr/VWTi catalyst and reducing N_2O formation. In addition, Cr and As usually coexist in the following industrial flue gases, such as coal- or biomass-fired boilers utilizing Cr/As-laden fuels, municipal solid waste incinerators, nonferrous metal smelting furnaces, and cement kilns, where high-temperature processes volatilize these heavy metals into the gas phase.[26−31] Therefore, the influence mechanism of the heavy metal As on the Cr/VWTi catalyst for the N_2O byproduct in the NH_3−SCR reaction deserves further investigation.

In this study, As−Cr-coloaded VWTi catalysts were synthesized using the actual concentrations of As and Cr from operational catalysts in order to investigate the effect of the As impurity on N_2O formation in Cr-poisoned VWTi catalysts during the NH_3−SCR reaction. The characterizations and DFT calculations revealed that the incorporation of the As impurity diminished oxygen vacancies, changed the monomeric VO_x configuration, and increased Brønsted acids in Cr-poisoned VWTi catalysts, which inhibited the deep dehydrogenation of absorbed NH_3, thus reducing the N_2O byproduct. This research provides novel insights into the suppression of N_2O by the effect of multiimpurities present in flue gas.

2. EXPERIMENTAL SECTION

2.1. Catalyst Preparation. The fresh VWTi catalyst was prepared via impregnation, and the content of V_2O_5 and WO_3 was 1 and 3 wt %, respectively. First, 25.7 mg of NH_4VO_3, 63.8 mg of $(NH_4)_{10}H_2W_{12}O_{42}\cdot 4H_2O$, and 55.4 mg of $H_2C_2O_4\cdot H_2O$ were dissolved in 100 mL of deionized water. Then, 1.92 g of anatase TiO_2 was added and stirred at room temperature for 4 h. Next, H_2O was removed from the suspension using an oil bath at 100 °C. Finally, the residue was dried at 100 °C for 12 h and then calcined in a muffle furnace at 500 °C for 4 h to obtain the VWTi catalyst.

All catalysts loaded with Cr and As were prepared by the wet impregnation method. The loading amounts of Cr and As were according to the actual industry content in the NH_3−SCR catalyst.[2,22,23,25] The fresh VWTi catalyst powder was added to the solutions of $Cr(NO_3)_3$, an As standard solution, and a mixture of both $Cr(NO_3)_3$ and the As standard solution, respectively. Then, the suspension was stirred at room temperature for 2 h. The subsequent preparation process was exactly the same as VWTi. The obtained samples were marked as Cr/VWTi, xAs/VWTi, and Cr-xAs/VWTi, where x means the molar ratio of As to V (when the molar ratio of As to V was 2, the samples were also marked as As/VWTi and As−Cr/VWTi). According to the reported spent catalysts,[2] the molar ratio of Cr to V was set to 0.1 for all samples.

2.2. NH_3−SCR Performance Test. The NH_3−SCR performance was evaluated in a fixed-bed quartz flow reactor with 0.1 g of the sample. The reaction gas contained 300 ppm of NH_3 (when used), 300 ppm of NO (when used), 4 vol % O_2 (when used), 100−200 ppm of SO_2 (when used), 5−10 vol % H_2O (when used), and Ar as the balanced gas (flow rate = 100 mL·min^{-1}, WHSV = 60,000 mL·g^{-1}·h^{-1}). After stabilization for 30 min at each temperature, the exhaust gas concentration was collected. The gas concentrations were monitored by an online ThermoFisher IS10 FTIR spectrometer. The data were collected when the SCR reaction was in a steady state at every temperature. The conversion was calculated using the following equation (NO_x includes NO and NO_2)

$$NO_x \text{ conversion } (\%) = \frac{[NO_x]_{in} - [NO_x]_{out}}{[NO_x]_{in}} \times 100\%$$

$$NH_3 \text{ conversion } (\%) = \frac{[NH_3]_{in} - [NH_3]_{out}}{[NH_3]_{in}} \times 100\%$$

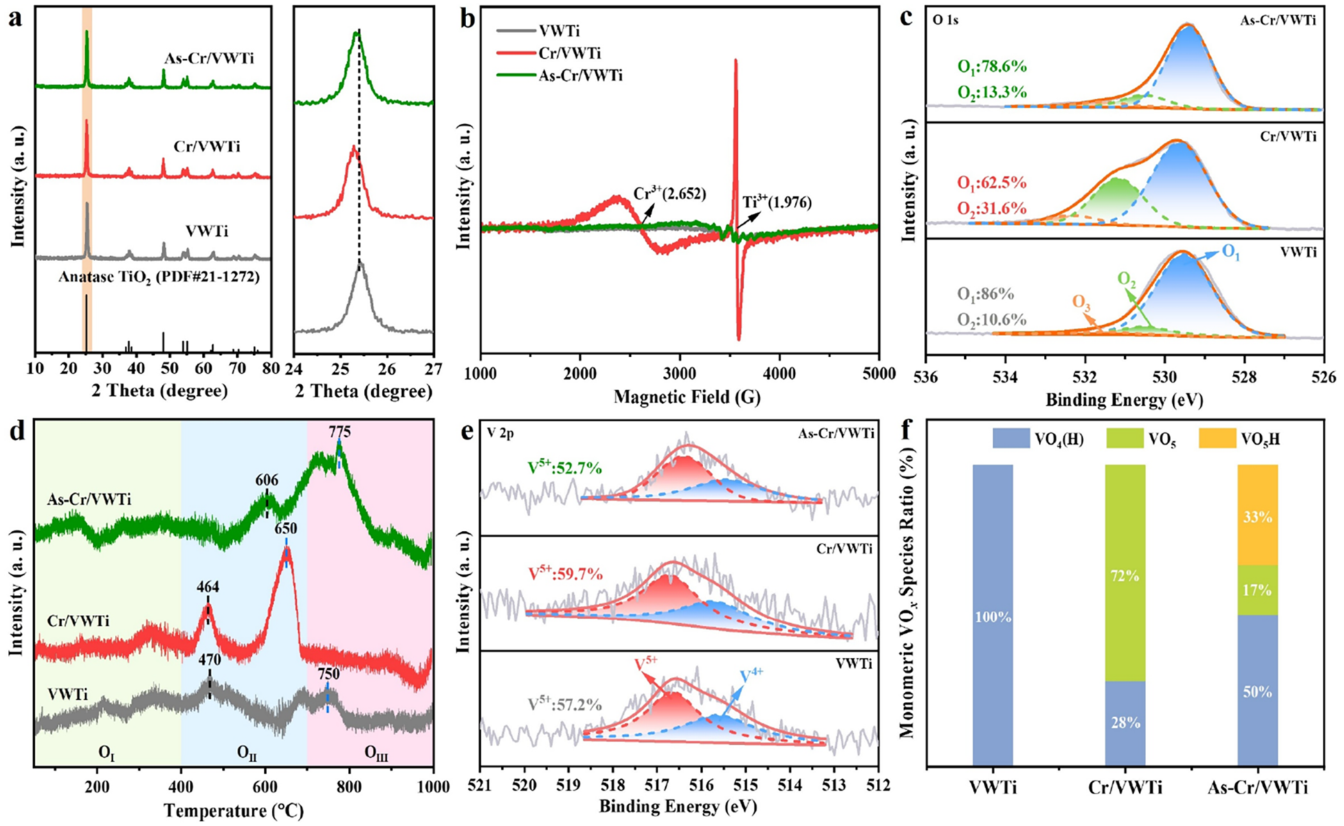

Figure 2. (a) XRD patterns. (b) EPR spectra. (c) XPS spectra of O 1s. (d) O_2-TPD (O_I (<400 °C): surface-adsorbed oxygen; O_{II} (400−700 °C): near-surface lattice oxygen; and O_{III} (>700 °C): bulk lattice oxygen). (e) XPS spectra of V 2p. (f) Relative content of monomeric vanadyl species by ^{51}V MAS NMR spectroscopy ($VO_4(H)$ represents the total content of VO_4 and VO_4H).

$$N_2 \text{ selectivity } (\%) = \left(1 - \frac{2[N_2O]_{out}}{[NH_3]_{in} + [NO_x]_{in} - [NH_3]_{out} - [NO_x]_{out}} \times 100\%\right)$$

2.3. Catalyst Characterization and Calculations. The detailed descriptions of the characterization methods and computational details are provided in the Supporting Information (SI).

3. RESULTS AND DISCUSSION

3.1. N_2O Formation in NH_3−SCR. Given the operating window of VWTi, the NH_3−SCR performance was evaluated in the temperature range from 300 to 450 °C. The NO_x conversion, N_2 selectivity, and N_2O concentration of VWTi, Cr/VWTi, xAs-Cr/VWTi, and 2As/VWTi (As/VWTi) are shown in Figure S1a−c. It was suggested that there was no significant change in the NO_x abatement performance of As/VWTi, 2As−Cr/VWTi (As−Cr/VWTi), Cr/VWTi, and VWTi catalysts. However, As−Cr/VWTi showed an obvious improvement in N_2 selectivity compared to Cr/VWTi. Specifically, within the temperature range of 300−400 °C, the N_2 selectivity of As−Cr/VWTi increased over 12%, and its N_2 selectivity equaled that of fresh VWTi at 300−350 °C. Moreover, the concentrations of the N_2O byproduct on Cr/VWTi and As−Cr/VWTi are depicted in Figure 1a. It could be found that at 300 °C, the N_2O yield on Cr/VWTi (40 ppm) was ten times that of As−Cr/VWTi catalysts (4 ppm). With the increased reaction temperature, more and more N_2O was produced on all catalysts, but the N_2O concentration was always in the order of Cr/VWTi > As−Cr/VWTi, suggesting that the introduction of the As impurity into the flue gas significantly suppressed the N_2O byproduct on Cr-poisoned VWTi in NH_3−SCR. In addition, as shown in Figure S1d−e, the As−Cr/VWTi catalyst exhibited excellent thermal stability.

In order to explore the origin of the N_2O byproduct, the possible N_2O formation pathways in the SI were investigated on Cr/VWTi and As−Cr/VWTi catalysts. Under the different reaction conditions (Figure S2), the results showed that negligible amounts of N_2O were produced under the conditions involving NH_3, NO + O_2, or NO, which suggested that the primary sources of N_2O formation in the NH_3−SCR reaction were the nonselective catalytic reduction (NSCR, eqs S1−S4) and NH_3 oxidation (eq S5) reactions on the Cr/VWTi and As−Cr/VWTi catalysts.[2] Then, the NO_x and NH_3 conversions under NH_3−SCR conditions on Cr/VWTi and As−Cr/VWTi were compared (Figure S3). It showed that from 300 to 400 °C, the NH_3 conversion remained at approximately 100%, whereas the NO_x conversion decreased by 10%. This indicated that as the temperatures were increased, more adsorbed NH_3 underwent oxidation rather than reacting with NO. Therefore, the NH_3 oxidation performance of Cr/VWTi and As−Cr/VWTi was evaluated at temperatures ranging from 300 to 400 °C (Figure S4). The N_2O concentrations of Cr/VWTi and As−Cr/VWTi gradually increased from near 0 to 40 and 19 ppm, respectively, with almost no other NO_x formation. On the basis of the above results, it was concluded that on both Cr/VWTi and As−Cr/VWTi, N_2O was predominantly generated from the NSCR reaction at 300 °C, while above 300 °C, the contribution of NH_3 oxidation to N_2O formation became increasingly significant, and the NH_3 oxidation process was more obvious on Cr/VWTi than on As−Cr/VWTi.

Commonly, H_2O and SO_2 are present in flue gas, and then N_2O formations under the conditions of 100−200 ppm of SO_2 and 5−10 vol % H_2O were determined on Cr/VWTi. It is seen in Figure S5 that the N_2O concentration exhibited a gradual decline with increasing SO_2 and H_2O concentrations. Subsequently, N_2O concentrations were measured for both Cr/VWTi and As−Cr/VWTi under mixed conditions of 100 ppm of SO_2 and 5 vol % H_2O. As shown in Figure 1b, at 350 °C, the combined presence of SO_2 and H_2O induced a significantly greater reduction in the N_2O concentration compared to either SO_2 or H_2O alone. Moreover, N_2O formation over the As−Cr/VWTi catalyst was found to be comparable to that over Cr/VWTi in the presence of 5 vol % H_2O. This suggested that the As impurity predominantly suppressed N_2O formation under actual operating conditions. Previous studies had shown that SO_2 or H_2O suppressed N_2O formation due to the introduction of Brønsted acid sites,[12,21] but the mechanism by which the As impurity inhibited N_2O formation over the Cr/VWTi catalyst remained unclear and required further detailed characterizations.

3.2. Oxygen Vacancies and VO_x Structures.

The crystal phases and pore structures of the catalysts were analyzed by XRD and BET, respectively. As shown in Figure 2a, all samples exclusively exhibited diffraction peaks corresponding to anatase-phase TiO_2 (PDF#21−1272), indicating that the deposition of Cr and As did not affect the crystal phases of the VWTi catalyst. Notably, there was a peak shift within the 24−27° range, which, for Cr/VWTi, shifted distinctly toward lower angles compared to pristine VWTi, suggesting the lattice expansion induced by Cr incorporation, whereas the peak of As−Cr/VWTi shifted toward higher angles, close to unloaded VWTi, indicating that As had inhibited the incorporation of Cr into the support lattice. According to the larger ionic radius of Cr^{3+} (0.615 Å) compared to Ti^{4+} (0.605 Å), the lattice expansion might be attributed to the substitution of Ti^{4+} by Cr^{3+} in Cr/VWTi. From the BET results (Table S1), there was no obvious change in the specific surface areas of As−Cr/VWTi, Cr/VWTi, and VWTi. Therefore, based on the XRD results, it was shown that Cr incorporates into the lattice of TiO_2, which was prevented in the As−Cr/VWTi catalyst.

In addition, EPR and XPS spectra were used to confirm the phenomenon. As shown in Figure 2b, besides the Ti^{3+} (g = 1.976) signal,[32] a new signal of g = 2.652 attributed to Cr^{3+} was observed in the Cr/VWTi sample.[33] However, only the Ti^{3+} signal was present in As−Cr/VWTi, clearly demonstrating that As inhibited the incorporation of Cr^{3+} into the TiO_2 lattice.

Moreover, the XPS spectra of Cr 2p and As 3d were analyzed. As shown in Figure S6a, the Cr 2p spectra displayed that two characteristic peaks at 578.6−579.8 and 575.9−577.1 eV were assigned to Cr^{6+} and Cr^{3+}, respectively.[34] It was found that the Cr^{3+} proportion in As−Cr/VWTi significantly decreased to 11.2 from 61.4% (Cr/VWTi). The pronounced decrease in the Cr^{3+} content of As−Cr/VWTi further suggested that As species prevented Cr into the TiO_2 lattice because the incorporation into TiO_2 usually led to the valence state similar to $Ti^{3+/4+}$ to maintain charge balance. In addition, as shown in Figure S6b, the As 3d peaks at 44.8−45.1 and 43.8−44.1 eV, attributed to As^{5+} and As^{3+}, respectively,[23] showed that there was an increase in the As^{5+} content in As−Cr/VWTi (86%) compared with As/VWTi (82.7%), which resulted from the oxidation of As^{3+} by Cr^{6+}, suggesting the interaction between Cr and As. As shown in Figure S7, the XPS spectrum of Ti 2p revealed that Cr/VWTi possessed the highest Ti^{3+} content, resulting from Cr-doping-induced lattice distortion in the TiO_2 lattice. However, upon As introduction, the Ti^{3+} content markedly declined, implying Cr segregation to the surface. Therefore, based on the XPS spectra of Cr 2p, As 3d, and Ti 2p, it was suggested that the introduction of As promoted the interaction between Cr and As, which prevented the incorporation of Cr into the TiO_2 lattice.

Generally, the incorporation into the lattice would result in lattice distortion, accompanied by the generation of oxygen vacancies, and thus the XPS spectra of O 1s and the O_2-TPD profile were used to detect the oxygen vacancies. As shown in Figure 2d, the XPS spectra of O 1s peaks at 529.4−529.7, 530.5−531.2, and 531.5−532.4 eV (marked as O_1, O_2, and O_3) could be assigned to lattice oxygen, oxygen chemisorbed on oxygen defects, and surface-adsorbed oxygen species, respectively.[32] Cr/VWTi displayed the highest content of the oxygen vacancy (31.6%), suggesting that Cr^{3+} occupied the original Ti^{4+} sites in the Cr/VWTi catalyst. In contrast, the incorporation of As remarkedly inhibited the formation of oxygen vacancies, resulting in its reduction of 18.3% compared to Cr/VWTi. In addition, the O_2-TPD profile is displayed in Figure 2d, and the O_2 desorption signals were assigned to surface-adsorbed oxygen (<400 °C, O_I), near-surface lattice oxygen (400−700 °C, O_{II}), and bulk lattice oxygen (>700 °C, O_{III}), respectively.[35] It could be observed that Cr deposition on the VWTi catalyst resulted in the peaks of near-surface lattice oxygen and bulk lattice oxygen shifting to lower temperatures, as well as the increased desorption peak areas. In contrast, the phenomenon of low-temperature shifts was not observed in the codeposition of As and Cr on the VWTi catalyst. This indicated that the oxygen mobility in Cr/VWTi was enhanced, compared with that in As−Cr/VWTi, which was attributed to oxygen vacancies caused by the lattice distortion.

Vanadium oxide, as the active component in VWTi catalysts, usually had an important influence on the N_2O byproduct from the NH_3 dehydrogenation in the NH_3−SCR reaction.[4,36,37] According to the reported findings,[2] the N_2O formation capability was directly related to the V^{5+} content in the V_2O_5/TiO_2 catalyst. Thus, we determined the XPS spectra of V 2p. As depicted in Figure 2e, the peaks at 516.4−516.8 and 515.4−515.7 eV were assigned to V^{5+} and V^{4+}, respectively.[2] The relative content of V^{5+} species was calculated from the fitted peak areas of V^{5+} and V^{4+}. It could be found that there was no obvious difference of the V^{5+} contents in VWTi and Cr/VWTi catalysts, which suggested that more N_2O formation on Cr/VWTi did not result from the valence states of VO_x species. Generally, the structure of VO_x species would significantly affect the activity and selectivity of NH_3−SCR.[36−39] We speculated that the differences in N_2O formation among the catalysts might come from changes in the VO_x structure.

Furthermore, the VO_x structure was explored by Raman and solid-state ^{51}V MAS NMR spectroscopies in order to explain the differences in N_2O formation on VWTi, Cr/VWTi, and As−Cr/VWTi. As shown in Figure S8, all catalysts exhibited the Raman characteristic bands for monomeric VO_x (1024, 1027 cm^{-1}) and tungstanyl W=O (1010 cm^{-1}).[35,37,38] It was

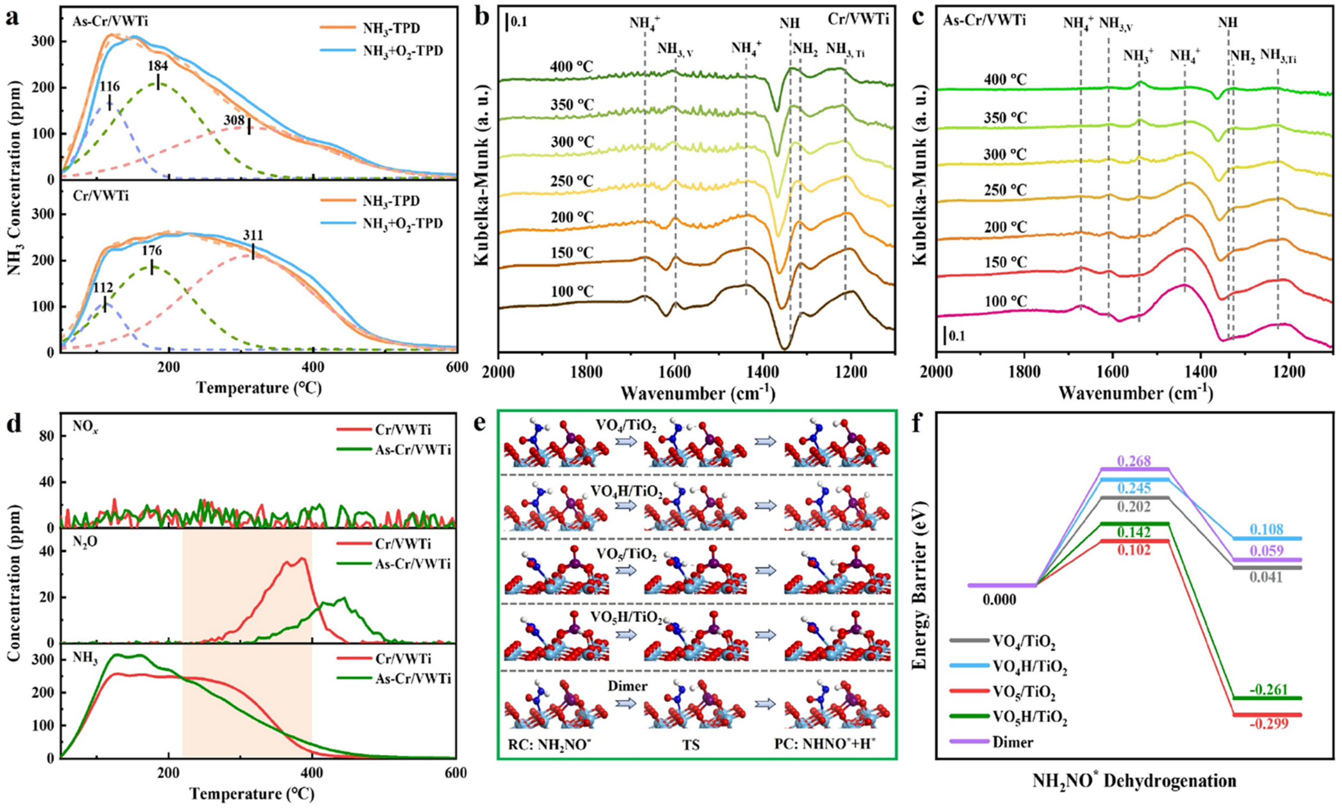

Figure 3. (a) NH_3 desorption signal during NH_3-TPD and NH_3 + O_2-TPD tests. *In situ* DRIFTS spectra of NH_3 adsorption over (b) Cr/VWTi and (c) As−Cr/VWTi in the temperature range of 100−400 °C, respectively. (d) NH_3 + O_2-TPSR profiles. (e) Dehydrogenation process on VO_4/TiO_2, VO_4H/TiO_2, VO_5/TiO_2, VO_5H/TiO_2, and the dimer (optimized geometries of the reactant (RC), transition state (TS), and product (PC) were presented; the asterisk (*) denotes the adsorbed state. Ti: light blue; V: purple; N: blue; O: red; H: white). (f) Calculated dehydrogenation energy barriers and energy changes of the reaction $NH_2NO^* \rightarrow NHNO^* + H^*$ on VO_4/TiO_2, VO_4H/TiO_2, VO_5/TiO_2, VO_5H/TiO_2, and the dimer.

noted that compared to VWTi, the monomeric VO_x characteristic band of Cr/VWTi underwent a red shift, while the introduction of As led to a blue shift compared to Cr/VWTi, which might be reported to the oxygen vacancies.[40] To obtain further insights into the vanadium species, we conducted ^{51}V MAS NMR analysis of the catalysts. As shown in Figure S9, compared to VWTi and Cr/VWTi, the peak (−442 ppm) of As−Cr/VWTi became more obvious, while the peak at −782 ppm nearly disappeared. This suggested that the As−Cr/VWTi sample contained more hydroxyl groups.[38,41,42] In order to clarify the VO_x configuration, based on the literature,[35,38,43−45] the ^{51}V MAS NMR spectra were fitted as shown in Figure S10, and the relative contents of the obtained VO_x species are summarized in Table S2. There were monomeric (VO_4(H), VO_5(H), VO_5), oligomerized, and bulk VO_x in VWTi, Cr/VWTi, and As−Cr/VWTi, where the abundance of monomeric VO_x species showed distinct structures and relative contents. As shown in Figure 2f, there were mainly VO_4(H) species in the VWTi catalyst; once the Cr deposition on the VWTi catalyst occurred, more than half of VO_4(H) species were transferred into VO_5 species. Moreover, the introduction of As on the Cr/VWTi catalyst caused over half of VO_5 to be converted into VO_4 and VO_5H species. The relative proportions of different monomeric VO_x species showed that only VO_4(H) species were present in VWTi, and Cr/VWTi exhibited the highest VO_5 species, while due to the interaction between As and Cr in As−Cr/VWTi, the VO_5H and VO_4(H) species were formed instead. In addition, it was observed that the content of oligomerized VO_x species in Cr/VWTi was 5.7% higher than that in As−Cr/VWTi.

On the basis of the above results of X-ray diffraction (XRD), electron paramagnetic resonance (EPR), X-ray photoelectron spectroscopy (XPS), O_2-TPD, Raman, and NMR characterizations, it could be inferred that the interaction of As−Cr prevented the incorporation of Cr^{3+} into the Cr/VWTi lattice, resulting in less oxygen vacancies and the changed VO_x species, which affected the NH_3−SCR performance.

3.3. NH_3 Adsorption and Dehydrogenation Analysis.

In the NH_3−SCR reaction, the catalyst's ability to absorb and activate NH_3 had influence on the N_2O formation.[11,12] Therefore, we conducted NH_3-TPD and NH_3 + O_2-TPD experiments on Cr/VWTi and As−Cr/VWTi to elucidate NH_3 adsorption. Figure 3a shows three deconvoluted NH_3-TPD peaks at ∼120, 180, and 310 °C, assigned to physisorbed NH_3, Brønsted acid-bound NH_3, and Lewis acid-bound NH_3, respectively.[35,36] It was seen from Table S3 that there are more Brønsted acid sites in As−Cr/VWTi and a higher content of Lewis acid sites in Cr/VWTi, consistent with the ^{51}V MAS NMR results. In addition, it was found that the Cr/VWTi or As−Cr/VWTi catalysts exhibited nearly similar NH_3 signals during the NH_3-TPD and NH_3 + O_2-TPD processes, which seemed to indicate that NH_3 was more adsorbed than O_2 on the two catalysts. Generally, the oxygen vacancy could adsorb O_2, and Cr/VWTi exhibited a higher oxygen vacancy content, but the profiles of NH_3-TPD and NH_3 + O_2-TPD of

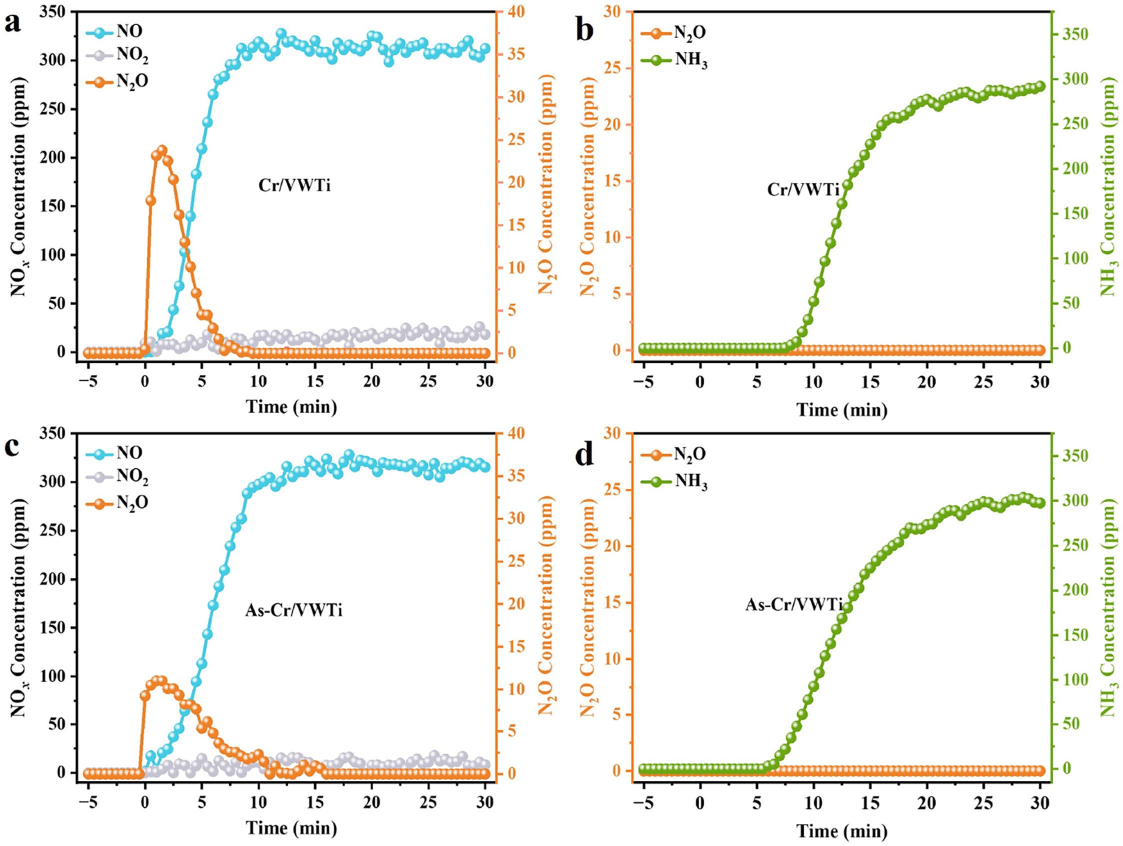

Figure 4. Transient reaction study. NO, NO_2, and N_2O concentrations in the outlet while passing NO + O_2 over NH_3-preabsorbed (a) Cr/VWTi and (c) As−Cr/VWTi at 300 °C. NH_3 concentrations in the outlet while passing NH_3 over NO_x-preabsorbed (b) Cr/VWTi and (d) As−Cr/VWTi at 300 °C.

Cr/VWTi were similar, which indicated that the oxygen vacancy acted as the adsorption site of NH_3.

In addition, the *in situ* DRIFTS spectra of NH_3 adsorption were taken in the temperature range of 100−400 °C to detect the NH_3 adsorption sites on the catalysts. As depicted in Figure 3b,c, the characteristic NH_3 adsorption vibrations observed at ca. 1215 cm^{-1} ($NH_{3,Ti}$) and ca. 1601 cm^{-1} ($NH_{3,V}$) were assigned to coordinated NH_3 bonded to the Ti site of V−O−Ti and the terminal V═O site, respectively.[36,46] The absorption bands at 1437 and 1668 cm^{-1} corresponded to NH_4^+ associated with Brønsted acid sites.[2] The negative absorption band observed at 1363 cm^{-1} was derived from NH_3 adsorption on sulfate species.[36] The peaks at ca. 1310 and 1541 cm^{-1} were attributed to NH_2 and NH_3^+ species, which were dehydrogenation products of coordinated NH_3 and NH_4^+, respectively.[2,22,23,47] The peak at 1338 cm^{-1} was ascribed to NH, resulting from the further dehydrogenation of NH_2.[2,47] It was found that the $NH_{3,Ti}$ signals were significantly higher than those of $NH_{3,V}$, indicating that the Ti sites next to the oxygen vacancies on the catalysts served as the main Lewis acid sites. Below 350 °C, the intensities of $NH_{3,Ti}$ and NH_4^+ signals were comparable on Cr/VWTi, whereas NH_4^+ significantly exceeded $NH_{3,Ti}$ on As−Cr/VWTi, suggesting a higher Brønsted acid content in As−Cr/VWTi, consistent with the results of ^{51}V MAS NMR and NH_3-TPD. Moreover, with the increased temperatures, the NH signal on Cr/VWTi became more pronounced, which on As−Cr/VWTi remained negligible, indicating that As−Cr/VWTi had a poorer capacity for NH_3 dehydrogenation than Cr/VWTi.

Furthermore, the NH_3 + O_2-TPSR experiments confirmed this phenomenon. As shown in Figure 3d, it was observed that in the reaction temperatures of 220−400 °C, As−Cr/VWTi showed less reduced NH_3 desorption and N_2O formation, as well as a higher temperature of N_2O formation compared to Cr/VWTi, indicating its weaker NH_3 adsorption and dehydrogenation ability. According to the report, oxygen vacancies could promote the adsorption and dehydrogenation of NH_3.[48,49] Therefore, combining the results of NH_3-TPD, NH_3 + O_2-TPD, *in situ* DRIFTS of NH_3 adsorption, and NH_3 + O_2-TPSR analyses, it could be concluded that less Lewis acid sites of Ti-oxygen vacancies in As−Cr/VWTi significantly reduced NH_3 adsorption and dehydrogenation abilities, in comparison with Cr/VWTi.

For the V_2O_5/TiO_2 catalyst, the dehydrogenation of NH_2NO to NHNO was the rate-limiting step in N_2O formation during NH_3−SCR.[4,10] The results of Raman and solid-state ^{51}V MAS NMR spectroscopies indicated that the introduction of As induced changes of the monomeric VO_x species in Cr/VWTi. To investigate the impact of different VO_x species on N_2O formation, we calculated the dehydrogenation energy barriers of NH_2NO^* to $NHNO^*$ intermediates on VO_4/TiO_2, VO_4H/TiO_2, VO_5/TiO_2, VO_5H/TiO_2, and the dimer (Table S4). As shown in Table S5, the adsorption energies of NH_2NO^* on the five configurations followed the order of VO_4/TiO_2 < VO_4H/TiO_2 < dimer < VO_5/TiO_2 < VO_5H/TiO_2, indicating that the absorption of NH_2NO^* on VO_4/TiO_2 species was the most stable. Moreover, the dehydrogenation process of NH_2NO^* over VO_4/TiO_2,

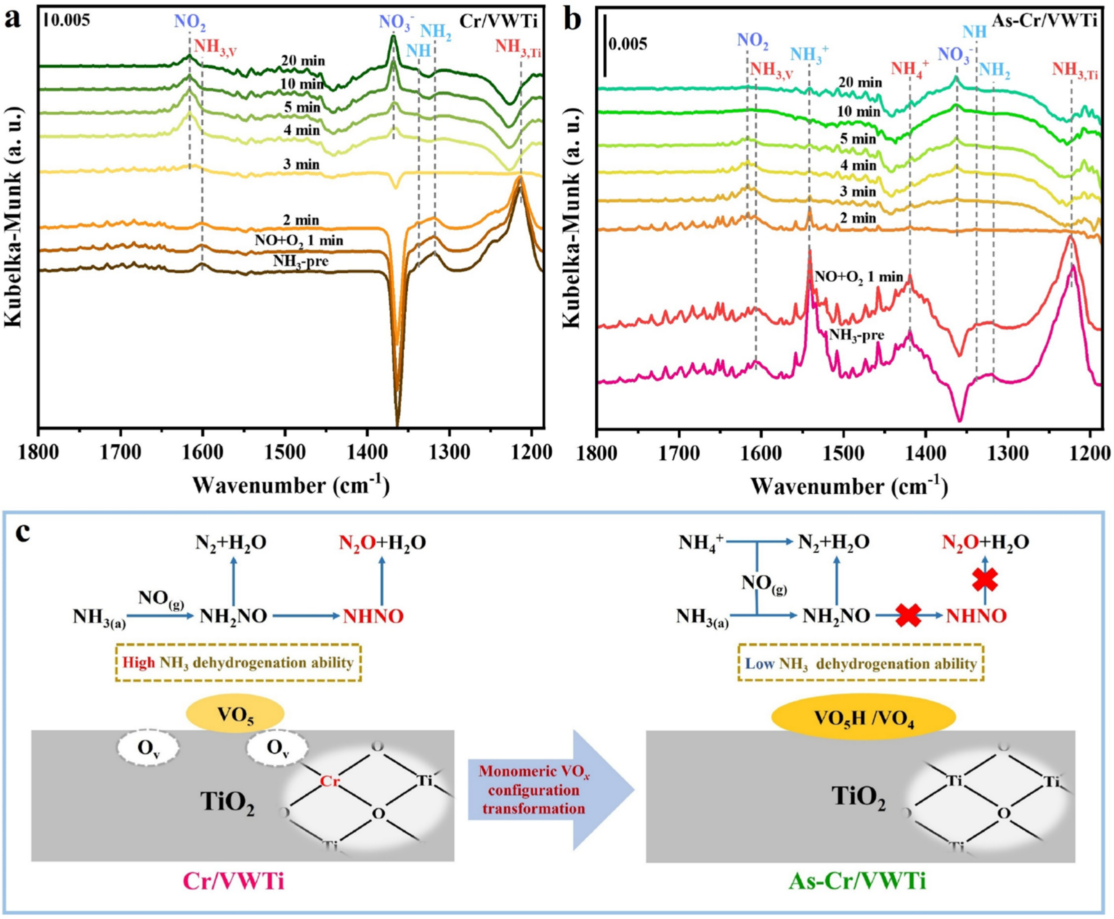

Figure 5. *In situ* DRIFTS spectra taken at 300 °C upon following NO + O_2 over NH_3-pretreated (a) Cr/VWTi and (b) As−Cr/VWTi. (c) Schematic illustration of As inhibiting N_2O formation on the Cr-poisoned VWTi catalyst in NH_3−SCR.

VO_4H/TiO_2, VO_5/TiO_2, VO_5H/TiO_2, and the dimer is illustrated in Figure 3e. The NH_2NO^* intermediate adsorbed at the Ti site, and then *H transferred to the oxygen of VO_x.[36] The energy changes during the dehydrogenation process are displayed in Figure 3f, and the dehydrogenation energy barriers of $NH_2NO^* \rightarrow NHNO^* + H^*$ on VO_4/TiO_2, VO_4H/TiO_2, VO_5/TiO_2, VO_5H/TiO_2, and the dimer were in the following order: $VO_5/TiO_2 < VO_5H/TiO_2 < VO_4/TiO_2 <$ dimer $< VO_4H/TiO_2$, suggesting that the dehydrogenation process of the NH_2NO^* intermediate on VO_5/TiO_2 species in Cr/VWTi was the easiest, leading to the highest N_2O generation.

Therefore, there was a decrease in the N_2O byproduct on As−Cr/VWTi, compared to Cr/VWTi, because of the reduced Lewis acid sites of Ti-oxygen vacancies for NH_3 adsorption and dehydrogenation, as well as the transformation of the VO_5 configuration (Cr/VWTi) to VO_4 and VO_5H (As−Cr/VWTi), making the dehydrogenation of the NH_2NO^* intermediate more difficult.

3.4. Reaction Mechanism of N_2O Formation.

To further explore the N_2O formation mechanism on Cr/VWTi and As−Cr/VWTi, the transient reaction experiments were performed at 300 °C. As shown in Figure 4a,4c, under the conditions of NH_3 preadsorption and the subsequent introduction of NO/O_2, the N_2O yield on Cr/VWTi was 2.2 times higher than that on As−Cr/VWTi. In contrast, under the reaction condition of NH_3 injection into NO_x preadsorption (Figure 4b,d), there is no N_2O formation on both the catalysts. Therefore, the generation of N_2O over both Cr/VWTi and As−Cr/VWTi followed the E-R pathway.

The reactive intermediate species usually could describe the mechanism of N_2O formation. Based on the E-R pathway, *in situ* DRIFTS spectra of NO + O_2 over NH_3-pretreated Cr/VWTi and As−Cr/VWTi catalysts were recorded at 300 °C. As depicted in Figure 5a,b, the NH species vanished in 3 min after the injection of NO and O_2, and the new bands assigned to NO_3^- (ca. 1367 cm^{-1}) and absorbed NO_2 (1616 cm $^{-1}$) appeared,[2] indicating the formation of N_2O from the NH and NO reaction on Cr/VWTi and As−Cr/VWTi.[10] The *in situ* DRIFTS of NH_3 adsorption demonstrated that the generation of NH over As−Cr/VWTi compared with Cr/VWTi was suppressed. Therefore, the lower N_2O formation over As−Cr/VWTi compared to Cr/VWTi could be attributed to its lower NH generation. Moreover, it could be observed that at 300 °C, As−Cr/VWTi exhibited a significant NH_4^+ signal and reacted with the introduced NO and O_2, whereas Cr/VWTi did not display an NH_4^+ signal. As reported, the NH_4^+ adsorbed on Brønsted acid sites generated N_2O via the further decomposition of ammonium nitrate, formed by its combination with NO_3^-.[12,21] However, as illustrated in Figure 4d, when NH_3 passed over As−Cr/VWTi preadsorbed with NO_x, no N_2O was produced, suggesting that NH_4^+ adsorbed on As−Cr/VWTi only yielded N_2. Therefore, the introduction of the As impurity into Cr/VWTi increased the content of Brønsted acids for NH_4^+ to N_2 formation and reduced the Lewis acid sites of oxygen vacancies and VO_5 species to make the intermediate dehydrogenation difficult, leading to a decrease in N_2O generation in the NH_3−SCR reaction (Figure 5c).

3.5. Environmental Implications. N_2O, as the third most important long-lived greenhouse gas, was found to generate a significant amount on the Cr-poisoned VWTi catalyst under practical NH_3−SCR working conditions. Herein, we proposed that the typical As impurity can significantly inhibit N_2O formation over the Cr/VWTi catalyst. The introduction of the As impurity effectively inhibited the incorporation of Cr into the TiO_2 lattice, reduced the formation of oxygen vacancies, facilitated the transformation of monomeric VO_x species (from VO_5 to VO_4 and VO_5H), and increased the Brønsted acids. Consequently, the NH_3 adsorption and excessive activation on the As−Cr/VWTi catalyst were weakened, inhibiting N_2O generation in the NH_3−SCR reaction. This work provides new insights into N_2O emission suppression via flue gas impurities.

ASSOCIATED CONTENT

Supporting Information

The Supporting Information is available free of charge at https://pubs.acs.org/doi/10.1021/acs.est.5c08985.

> Information about catalyst characterization, calculations, and the N_2O formation pathway (Text S1); surface area and pore structure (Table S1); relative content of different vanadyl species (Table S2); NH_3 desorption during NH_3-TPD tests (Table S3); the calculated dehydrogenation energy changes of NH_2NO on VO_x/TiO_2 surfaces (Table S4); the adsorption energy of NH_2NO adsorbed on VO_x/TiO_2 surfaces (Table S5); NH_3−SCR performances (Figure S1); N_2O formation of Cr/VWTi and As−Cr/VWTi in different reactions (Figure S2); NH_3/NO_x conversion of Cr/VWTi and As−Cr/VWTi in the NH_3−SCR reaction (Figure S3); NH_3 conversion and NO_x/N_2O concentration in the reaction of NH_3 + O_2 (Figure S4); NH_3−SCR performances with SO_2 and H_2O at 350 °C (Figure S5); XPS spectra of Cr 2p and As 3d (Figure S6); XPS spectra of Ti 2p (Figure S7); Raman spectra (Figure S8); the complete ^{51}V MAS NMR spectra (Figure S9); ^{51}V MAS NMR spectroscopy results in the center-band region (Figure S10); and VO_x/TiO_2 models (Figure S11) (PDF)

AUTHOR INFORMATION

Corresponding Authors

Weixin Zou − *School of Atmospheric Sciences, State Key Laboratory of Water Pollution Control and Green Resource Recycling, School of Environment, Jiangsu Key Laboratory of Vehicle Emissions Control, Nanjing University, Nanjing 210093, P. R. China;* orcid.org/0000-0001-5001-2841; Email: wxzou2016@nju.edu.cn

Lin Dong − *School of Atmospheric Sciences, State Key Laboratory of Water Pollution Control and Green Resource Recycling, School of Environment, Jiangsu Key Laboratory of Vehicle Emissions Control, Nanjing University, Nanjing 210093, P. R. China;* orcid.org/0000-0002-8393-6669; Email: donglin@nju.edu.cn

Authors

Ruihua Wang − *School of Atmospheric Sciences, State Key Laboratory of Water Pollution Control and Green Resource Recycling, School of Environment, Jiangsu Key Laboratory of Vehicle Emissions Control, Nanjing University, Nanjing 210093, P. R. China*

Ziyi Fan − *School of Atmospheric Sciences, State Key Laboratory of Water Pollution Control and Green Resource Recycling, School of Environment, Jiangsu Key Laboratory of Vehicle Emissions Control, Nanjing University, Nanjing 210093, P. R. China*

Jingtao Wang − *School of Atmospheric Sciences, State Key Laboratory of Water Pollution Control and Green Resource Recycling, School of Environment, Jiangsu Key Laboratory of Vehicle Emissions Control, Nanjing University, Nanjing 210093, P. R. China*

Zhisu Liu − *Suzhou Environmental Monitoring Station, Suzhou 215000, P. R. China*

Hao Cheng − *Nantong Ecological Environment Monitoring Center, Nantong 226000, P. R. China*

Xingshen Yang − *Yangzhou Sanfang Testing Technology Co., Ltd., Yangzhou 225000, P. R. China*

Wei Nie − *School of Atmospheric Sciences, State Key Laboratory of Water Pollution Control and Green Resource Recycling, School of Environment, Jiangsu Key Laboratory of Vehicle Emissions Control, Nanjing University, Nanjing 210093, P. R. China; Joint International Research Laboratory of Atmospheric and Earth System Research, School of Atmospheric Sciences, Nanjing University, Nanjing 210023, P. R. China; National Observation and Research Station for Atmospheric Processes and Environmental Change in Yangtze River Delta, Nanjing 210023, P. R. China;* orcid.org/0000-0002-6048-0515

Complete contact information is available at: https://pubs.acs.org/10.1021/acs.est.5c08985

Notes

The authors declare no competing financial interest.

ACKNOWLEDGMENTS

This work was supported by the National Natural Science Foundation of China (62375120, 22476085, and 22106067) and the Natural Science Foundation of Jiangsu Province of China (BK20240171 and BK20231513).

REFERENCES

(1) Tang, C. J.; Zhang, H. L.; Dong, L. Ceria-based catalysts for low-temperature selective catalytic reduction of NO with NH_3. *Catal. Sci. Technol.* **2016**, *6* (5), 1248−1264.

(2) Xing, J. Y.; Xue, Q. T.; Chen, J. J.; Mi, J. X.; Chen, X. P.; Shi, J. Q.; Liu, Z. M.; Li, J. H. Potential risk of significant N_2O emission without changing NO_x conversion on commercial V_2O_5/TiO_2 catalyst under working conditions. *Environ. Sci. Technol.* **2023**, *57* (51), 21866−21875.

(3) Duan, R. C.; Fu, Y.; Li, Z. C.; Wang, X.; Gao, M.; Yu, Y. B.; He, G. Z.; He, H. Unexpected room-temperature selective catalytic reduction of NO_x with NH_3 over metal-free carbon-based catalysts. *Environ. Sci. Technol.* **2025**, *59* (15), 7760−7767.

(4) Wang, X. M.; Du, X. S.; Xue, J. Y.; Yang, G. P.; Chen, Y. R.; Zhang, L. New insights into the N_2O formation mechanism during selective catalytic reduction of NO_x with NH_3 over V-based catalyst. *Catal. Today* **2020**, *355*, 555−562.

(5) Li, L.; Xu, J. H.; Hu, J. X.; Han, J. R. Reducing nitrous oxide emissions to mitigate climate change and protect the ozone layer. *Environ. Sci. Technol.* **2014**, *48* (9), 5290−5297.

(6) Janssen, F. J. J. G.; Vandenkerkhof, F. M. G.; Bosch, H.; Ross, J. R. H. Mechanism of the reaction of nitric-oxide, ammonia, and

oxygen over vanadia catalysts. 2. isotopic transient studies with O-18 and N-15. *J. Phys. Chem. A* **1987**, *91* (27), 6633−6638.

(7) Ozkan, U. S.; Cai, Y. P.; Kumthekar, M. W. Mechanistic studies of selective catalytic reduction of nitric-oxide with ammonia over V_2O_5/TiO_2 (anatase) catalysts through transient isotopic labeling at steady-state. *J. Phys. Chem. A* **1995**, *99* (8), 2363−2371.

(8) Ozkan, U. S.; Kumthekar, M. W.; Cai, Y. P. P. Selective catalytic reduction of nitric-oxide over vanadia/titania catalysts-temperature-programmed desorption and isotopically labeled oxygen-exchange studies. *Ind. Eng. Chem. Res.* **1994**, *33* (12), 2924−2929.

(9) Zhu, M. H.; Lai, J. K.; Wachs, I. E. Formation of N_2O greenhouse gas during SCR of NO with NH_3 by supported vanadium oxide catalysts. *Appl. Catal. B: Environ.* **2018**, *224*, 836−840.

(10) Gao, M.; Li, Z. C.; He, G. Z.; Shan, Y. L.; Sun, Y.; He, H. Unveiling the origin of selectivity in the selective catalytic reduction of NO with NH_3 over oxide catalysts. *Environ. Sci. Technol.* **2023**, *57* (22), 8426−8434.

(11) Ko, S. J.; Tang, X. L.; Gao, F. Y.; Yi, H. H.; Liu, H. H.; Luo, N. Remarkable N_2-selectivity enhancement of NH_3-SCR over HPMo modified MnCo-BTC@SiO_2 catalyst. *J. Environ. Sci.* **2024**, *138*, 482−495.

(12) Li, J. C.; Zhang, C.; Fang, D. L.; Zheng, Z.; Zhao, Y.; Tan, P.; Fang, Q. Y.; Chen, G. The inhibition mechanism of N_2O generation in NH_3-SCR process by water vapor. *J. Hazard. Mater.* **2025**, *485*, No. 136881.

(13) Zhang, P.; Wang, P. L.; Impeng, S.; Lan, T. W.; Liu, X. Y.; Zhang, D. S. Unique compensation effects of heavy metals and phosphorus copoisoning over NO_x reduction catalysts. *Environ. Sci. Technol.* **2022**, *56* (17), 12553−12562.

(14) Wei, X. L.; Ke, Q. L.; Cheng, H.; Guo, Y.; Yuan, Z. S.; Zhao, S. S.; Sun, T. J.; Wang, S. D. Seed-assisted synthesis of Cu-(Mn)-UZM-9 zeolite as excellent NO removal and N_2O inhibition catalysts in wider temperature window. *Chem. Eng. J.* **2020**, *391*, No. 123491.

(15) Cao, J.; Rohani, S.; Liu, W. Z.; Liu, H. H.; Lu, Z. Q.; Wu, H. L.; Jiang, L. J.; Kong, M.; Liu, Q. C.; Yao, X. J. Influence of phosphorus on the NH_3-SCR performance of CeO_2-TiO_2 catalyst for NO_x removal from co-incineration flue gas of domestic waste and municipal sludge. *J. Colloid Interface Sci.* **2022**, *610*, 463−473.

(16) Li, Y. S.; Leng, X. S.; Zhang, Z. P.; Niu, X. Y.; Zhu, Y. J. Modulating NH_3 oxidation and inhibiting sulfate deposition to improve NH_3-SCR denitration performance by controlling Mn/Nb ratio over $Mn_aNbTi_2O_x$ (a = 0.6−0.9) catalysts. *J. Hazard. Mater.* **2025**, *482*, 136568.

(17) Wang, X. F.; Zhao, Z.; Xu, Y.; Li, Q. B. Promoting effect of Ti addition on three-dimensionally ordered macroporous Mn-Ce catalysts for NH_3-SCR reaction: enhanced N_2 selectivity and remarkable water resistance. *Appl. Surf. Sci.* **2021**, *569*, No. 151047.

(18) Huang, Y. Q.; Li, P. X.; Zhang, R. D.; Wei, Y. Efficiency of phosphotungstic acid modified Mn-based catalysts to promote activity and N_2 formation for selective catalytic reduction of NO with ammonia. *Int. J. Chem. React. Eng.* **2019**, *17* (7), No. 20180057.

(19) Chen, L.; Yao, X. J.; Cao, J.; Yang, F. M.; Tang, C. J.; Dong, L. Effect of Ti^{4+} and Sn^{4+} co-incorporation on the catalytic performance of CeO_2-MnO_x catalyst for low temperature NH_3-SCR. *Appl. Surf. Sci.* **2019**, *476*, 283−292.

(20) Liu, T.; Su, S.; Liu, L. J.; Yu, Q.; Xu, K.; Jiang, L.; Xu, J.; Wang, Y.; Hu, S.; Xiang, J. Mechanistic investigation of the suppressed N_2O formation during the low-temperature NH_3-SCR over the Sb-modified Mn/Ti catalyst. *Chem. Eng. J.* **2024**, *499*, No. 156301.

(21) Zhang, B. L.; Liebau, M.; Suprun, W.; Liu, B.; Zhang, S. G.; Gläser, R. Suppression of N_2O formation by H_2O and SO_2 in the selective catalytic reduction of NO with NH_3 over a Mn/Ti-Si catalyst. *Catal. Sci. Technol.* **2019**, *9* (17), 4759−4770.

(22) Peng, Y.; Li, J. H.; Si, W. Z.; Luo, J. M.; Dai, Q. Z.; Luo, X. B.; Liu, X.; Hao, J. M. Insight into deactivation of commercial SCR catalyst by arsenic: an experiment and DFT study. *Environ. Sci. Technol.* **2014**, *48* (23), 13895−13900.

(23) Li, X.; Li, J. H.; Peng, Y.; Si, W. Z.; He, X.; Hao, J. M. Regeneration of commercial SCR catalysts: probing the existing forms of arsenic oxide. *Environ. Sci. Technol.* **2015**, *49* (16), 9971−9978.

(24) Jiang, S.; Su, Q. F.; Yin, Y.; Zhu, T. L.; Li, X. Extraordinary detoxification effect of arsenic on the cadmium- poisoned V_2O_5/TiO_2 catalyst for selective catalytic reduction of NO_x by NH_3. *ACS EST Eng.* **2023**, *3* (5), 725−733.

(25) Lu, Q.; Pei, X. Q.; Wu, Y. W.; Xu, M. X.; Liu, D. J.; Zhao, L. Deactivation mechanism of the commercial V_2O_5-MoO_3/TiO_2 selective catalytic reduction catalyst by arsenic poisoning in coal-fired power plants. *Energy Fuels* **2020**, *34* (4), 4865−4873.

(26) Tong, Y. L.; Gao, J. J.; Yue, T.; Zhang, X. X.; Liu, J. Y.; Bai, J. Distribution, chemical fractionation, and potential environmental risks of Hg, Cr, Cd, Pb, and As in wastes from ultra-low emission coal-fired industrial boilers in China. *J. Hazard. Mater.* **2023**, *446*, No. 130606.

(27) Wang, H. Y.; Ma, Z. R.; Li, G.; Ma, J.; Zhao, C. L.; Zhou, J. L.; Wang, L.; Peng, S. P. Research progress in synergistic catalytic elimination of multiple pollutants in flue gas of coal combustion coupled with renewable fuels. *Chem. Ind. Eng. Prog.* **2024**, *43* (4), 1783−1795.

(28) Jia, W. K.; Guo, Y.; Guo, F. H.; Li, H. C.; Li, Y.; Zhang, Y. X.; Wu, J. J.; Si, C. D. Co-combustion of carbon-rich fraction from coal gasification fine slag and biochar: Gas emission, ash sintering, heavy metals evolutions and environmental risk evaluation. *Chem. Eng. J.* **2023**, *471*, No. 144312.

(29) Chuai, X.; Xiao, R. H.; Chang, L.; Wang, J.; Yong, H.; Jiang, R. Y.; Zhang, T. L.; Tan, S. T.; Zhao, Y. C.; Xiong, Z.; Zhang, J. Y. Fate and emission behavior of heavy metals during hazardous chemical waste incineration. *J. Hazard. Mater.* **2022**, *431*, No. 128656.

(30) Zhang, J. W.; Sun, X. H.; Deng, J. G.; Li, G. L.; Li, Z. J.; Jiang, J. K.; Wu, Q. R.; Duan, L. Emission characteristics of heavy metals from a typical copper smelting plant. *J. Hazard. Mater.* **2022**, *424*, No. 127311.

(31) Yang, Z. Z.; Chen, Y.; Sun, Y. Q.; Liu, L. L.; Zhang, Z. T.; Ge, X. L. The partitioning behavior of trace element and its distribution in the surrounding soil of a cement plant integrated utilization of hazardous wastes. *Environ. Sci. Pollut. Res.* **2016**, *23* (14), 13943−13953.

(32) Ou, G.; Xu, Y. S.; Wen, B.; Lin, R.; Ge, B. H.; Tang, Y.; Liang, Y. W.; Yang, C.; Huang, K.; Zu, D.; Yu, R.; Chen, W. X.; Li, J.; Wu, H.; Liu, L. M.; Li, Y. D. Tuning defects in oxides at room temperature by lithium reduction. *Nat. Commun.* **2018**, *9*, No. 1302.

(33) Dvoranová, D.; Brezová, V.; Mazúr, M.; Malati, M. A. Investigations of metal-doped titanium dioxide photocatalysts. *Appl. Catal. B: Environ.* **2002**, *37* (2), 91−105.

(34) Li, S. J.; Wang, X. X.; Tan, S.; Shi, Y.; Li, W. CrO_3 supported on sargassum-based activated carbon as low temperature catalysts for the selective catalytic reduction of NO with NH_3. *Fuel* **2017**, *191*, 511−517.

(35) Long, Y. P.; Su, Y. T.; Chen, M. L.; Lu, S.; Luo, X. Q.; Zhu, Z. H.; Wu, Z. B.; Weng, X. L. Polymerization state of vanadyl species affects the catalytic activity and arsenic resistance of the V_2O_5-WO_3/TiO_2 catalyst in multipollutant control of NO_x and chlorinated aromatics. *Environ. Sci. Technol.* **2023**, *57* (19), 7590−7598.

(36) He, G. Z.; Lian, Z. H.; Yu, Y. B.; Yang, Y.; Liu, K.; Shi, X. Y.; Yan, Z. D.; Shan, W. P.; He, H. Polymeric vanadyl species determine the low-temperature activity of V-based catalysts for the SCR of NO_x with NH_3. *Sci. Adv.* **2018**, *4* (11), No. eaau4637.

(37) Lian, Z. H.; Wei, J.; Shan, W. P.; Yu, Y. B.; Radjenovic, P. M.; Zhang, H.; He, G. Z.; Liu, F. D.; Li, J. F.; Tian, Z. Q.; He, H. Adsorption-induced active vanadium species facilitate excellent performance in low-temperature catalytic NO_x abatement. *J. Am. Chem. Soc.* **2021**, *143* (27), 10454−10461.

(38) Jaegers, N. R.; Lai, J.-K.; He, Y.; Walter, E.; Dixon, D. A.; Vasiliu, M.; Chen, Y.; Wang, C. M.; Hu, M. Y.; Mueller, K. T.; Wachs, I. E.; Wang, Y.; Hu, J. Z. Mechanism by which tungsten oxide promotes the activity of supported V_2O_5/TiO_2 catalysts for NO_x abatement: structural effects revealed by ^{51}V MAS NMR spectroscopy. *Angew. Chem., Int. Ed.* **2019**, *58* (36), 12609−12616.

(39) Song, I.; Youn, S.; Lee, H.; Lee, S. G.; Cho, S. J.; Kim, D. H. Effects of microporous TiO_2 support on the catalytic and structural properties of V_2O_5 microporous TiO_2 for the selective catalytic reduction of NO by NH_3. *Appl. Catal. B: Environ.* **2017**, *210*, 421−431.

(40) An, D.; Yang, S.; Cheng, Q. N.; Yan, W. T.; Sun, J. F.; Zou, W. X.; Sun, C. Z.; Tang, C. J.; Dong, L. Water-driven surface lattice oxygen activation in MnO_2 for promoted low-temperature NH_3-SCR. *Environ. Sci. Technol.* **2024**, *58* (38), 16974−16983.

(41) Eckert, H.; Wachs, I. E. Solid-state ^{51}V NMR structural studies on supported vanadium(V) oxide catalysts- vanadium-oxide surface-layers on alumina and titania supports. *J. Phys. Chem. A* **1989**, *93* (18), 6796−6805.

(42) Epifani, M.; Diaz, R.; Force, C.; Comini, E.; Andreu, T.; Zamani, R. R.; Arbiol, J.; Siciliano, P.; Faglia, G.; Morante, J. R. Colloidal counterpart of the TiO_2-supported V_2O_5 system: a case sudy of oxide-on-oxide deposition by wet chemical techniques. synthesis, vanadium speciation, and gas-sensing enhancement. *J. Phys. Chem. C* **2013**, *117* (40), 20697−20705.

(43) Hu, J. Z.; Xu, S. C.; Li, W. Z.; Hu, M. Y.; Deng, X. C.; Dixon, D. A.; Vasiliu, M.; Craciun, R.; Wang, Y.; Bao, X. H.; Peden, C. H. F. Investigation of the structure and active sites of TiO_2 nanorod supported VO_x catalysts by high-field and fast-spinning ^{51}V MAS NMR. *ACS Catal.* **2015**, *5* (7), 3945−3952.

(44) Lai, J. K.; Jaegers, N. R.; Lis, B. M.; Guo, M. Y.; Ford, M. E.; Walter, E.; Wang, Y.; Hu, J. Z.; Wachs, I. E. Structure-activity relationships of hydrothermally aged titania-supported vanadium-tungsten oxide catalysts for SCR of NO_x emissions with NH_3. *ACS Catal.* **2021**, *11* (19), 12096−12111.

(45) Jaegers, N. R.; Wang, Y.; Hu, J. Z.; Wachs, I. E. Impact of hydration on supported V_2O_5/TiO_2 catalysts as explored by magnetic resonance spectroscopy. *J. Phys. Chem. C* **2021**, *125* (30), 16766−16775.

(46) Lv, Z.; He, G. Z.; Ge, Y. L.; Liu, Y. C.; Yu, Y. B.; He, H. Effects of WO_3 and MoO_3 loadings on vanadia-based catalysts for NH_3-SCR: Revealed by in situ infrared and two-dimensional correlation spectroscopy. *Fuel* **2024**, *359*, No. 130472.

(47) Amores, J. M. G.; Escribano, V. S.; Ramis, G.; Busca, G. An FT-IR study of ammonia adsorption and oxidation over anatase-supported metal oxides. *Appl. Catal. B: Environ.* **1997**, *13* (1), 45−58.

(48) Li, G.; Wang, B. D.; Ma, Z. R.; Ma, J.; Wang, H. Y.; Zhou, J. L.; Peng, S. P.; White, J. J.; Li, Y. L.; Chen, J. Y.; Han, Z. H.; Wei, H.; Peng, C.; Xiong, Y. J.; Wang, Y. An anti-poisoning defective catalyst without metal active sites for NH_3-SCR via *in situ* stabilization. *EES Catal.* **2023**, *1*, 134−143.

(49) Wang, R. H.; Hao, Z. F.; Huang, X.; Peng, Y.; Liu, G. Q.; Xia, Y. G.; Zhan, S. H. In-situ formation of carbon-doped cerium-zirconium solid solution as a superacid catalyst for the removal of NO_x. *Appl. Catal. B: Environ.* **2023**, *339*, No. 123098.